Analytical Model for the Characterization of the Guiding Zone Tribotest for Tube Hydroforming

Gracious Ngaile

Chen Yang

Department of Mechanical and Aerospace Engineering,
North Carolina State University,
Campus Box 7910,
Raleigh, NC 27695

Common part failures in tube hydroforming include wrinkling, premature fracture, and unacceptable part surface quality. Some of these failures are attributed to the inability to optimize tribological conditions. There has been an increasing demand for the development of effective lubricants for tube hydroforming due to widespread application of this process. This paper presents an analytical model of the guiding zone tribotest commonly used to evaluate lubricant performance for tube hydroforming. Through a mechanistic approach, a closed-form solution for the field variables contact pressure, effective stress/strain, longitudinal stress/strain, and hoop stress can be computed. The analytical model was validated by the finite element method. In addition to determining friction coefficient, the expression for local state of stress and strain on the tube provides an opportunity for in-depth study of the behavior of lubricant and associated lubrication mechanisms. The model can aid as a quick tool for iterating geometric variables in the design of a guiding zone, which is an integral part of tube hydroforming tooling. [DOI: 10.1115/1.3090888]

Keywords: tribotest, friction coefficient, tube hydroforming, closed-form equations

1 Introduction

Tube hydroforming (THF) is a process of manufacturing intricate shapes from tubular blanks. A hydraulic fluid is pressurized inside the tube to a yield point, hence forcing the blank to conform to the die shape. To increase shaping capability, the tubular blank ends are usually fed toward the die cavity during pressurization. Tube hydroforming has gained wide acceptance in the automotive and aerospace industries due to its advantages over stamping, such as part consolidation, weight reduction, higher part quality, fewer secondary operations, improved structural strength, and increased stiffness [1–4].

Better understanding of tribological aspects in THF is imperative for advancement of this technology. Common failures in THF include wrinkling, premature fracture, and unacceptable part surface quality [5,6]. Some of these failures are attributed to either utilizing ineffective lubrication/lubricant or failure to optimize tribological conditions in the process design. THF can be categorized into three friction zones: the guiding zone, the transition zone, and the expansion zone (Fig. 1). Research has shown that the three friction zones exhibit different states of stress [7,8]. These stress differences, which also imply different lubrication mechanisms, have led to the development of tribotests that can be used to study numerous tribological aspects in THF [8–12]. This includes (a) screening of new lubricants that can perform well in the three friction zones, (b) determination of friction coefficient via tribotest for use in numerical modeling, and (c) determination of wear characteristics of the dies used.

Three variants of tribotests are normally used for the guiding zone, as shown in Fig. 2. All of these tests involve pressurizing the tubular specimen to the required pressure level and pushing the tube through a cylindrical die.

Variant I was originally developed at the University of Darmstadt in collaboration with Schuler [8]. In this test, the normal load is measured via a load cell connected to the upper half of the die. Applying Coulomb's law, the interface friction coefficient can be determined by Eq. (1). Friction force, F_f, and normal load, F_c, are both measured by load cells connected to the system. To facilitate measurement of F_c, split die system is used.

$$\mu = \frac{F_f}{F_C} \tag{1}$$

This test requires careful design of the tooling to ensure that energy flow in the system components does not result in significant errors in the measurement of the normal load.

Variant II was originally developed at the Engineering Research Center for Net Shape Manufacturing at the Ohio State University [13,14]. In this test, the vertical shaft that holds the tube is connected to a load cell that measures the frictional force, F_f. Unlike variant I, the normal load in this test is determined indirectly using the internal pressure of the tube and the properties of the tube material. The friction coefficient is determined by

$$\mu = \frac{cF_f}{P_i \pi \mathrm{Di} L} \tag{2}$$

where F_f is the friction force, P_i is the internal pressure in the tube, Di is the internal diameter of the tube, L is the effective length of the tube, and c is a constant. Accurate determination of c is critical. For higher pressure and tubular specimens with higher diameter-to-wall thickness ratios, the value of c will approach 1.

Variant III, developed at the University of Paderborn [15,16], differs from variant II in how the friction force is determined. In this test, two punches are connected to the tube ends. These punches are connected to separate load cells to measure the friction force. This test allows emulation of the compression of a tube being pushed through a die. The friction force is determined by taking the difference in the friction loads measured by the two load cells. The friction coefficient can be determined by Eq. (3). The test assumes that the internal pressure is equal to the pressure

Contributed by the Manufacturing Engineering Division of ASME for publication in the JOURNAL OF MANUFACTURING SCIENCE AND ENGINEERING. Manuscript received June 25, 2008; final manuscript received December 31, 2008; published online March 18, 2009. Review conducted by Jian Cao.

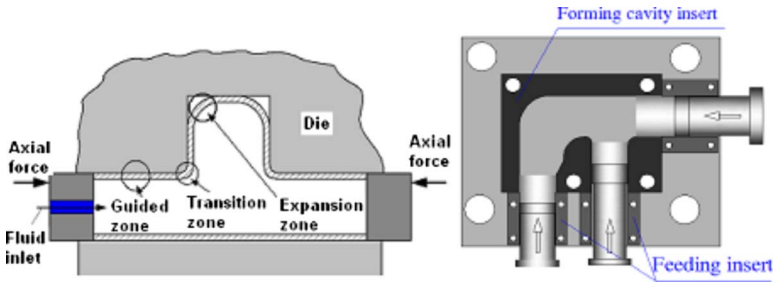

Fig. 1 (*a*) Friction zone in THF; (*b*) typical THF tooling

at the tool-workpiece interface. In reality, the interface pressure may vary drastically depending on the friction level and geometric variables.

$$\mu = \frac{F_1 - F_2}{P_i \pi \mathrm{Di} L} \tag{3}$$

While all of the test variants discussed above can be used to rank lubricants effectively, they cannot accurately determine interface pressure distribution, which is a vital parameter for accurate determination of friction coefficient as well as for studying other tribological aspects at the interface, such as the wear rate of the tools.

2 Objectives and Approach

The objectives of this paper are to (a) establish a closed-form solution that describes the principal stress state and strain state of a tube that is pushed through a die under internal pressure loading, and (b) formulate a closed-form solution that will facilitate determination of contact pressure at the tool-tube interface and in turn make possible to accurately determine interface friction based on Coulomb's law. The derived equations should also be valuable in designing guiding zones where variations in the interface pressure loading are a function of interface friction and the ratio between tube length and tube diameter. The analytical model will also bring about better understanding of the severity of deformation at the tool-workpiece interface as the state of stress/strain varies along the tube length.

The derivation commences by establishing expressions for the principal stresses and strains acting on a plastically deformed tubular material that is being pushed along a die under constant internal pressure P_i. These are radial stress σ_r, longitudinal stress σ_z, hoop stress σ_h, longitudinal strain ε_z, and radial strain ε_r. Hoop strain, ε_θ, is assumed to be zero because the tube is constrained by the die. Effective stress and effective strain are established based on von Mises yield criteria, and the deforming tubular material is assumed to follow the power law, $\bar{\sigma} = K\bar{\varepsilon}^n$, where $\bar{\sigma}$ is the flow stress, K is the strength coefficient, $\bar{\varepsilon}$ is the effective strain, and n is the strain hardening exponent. After the state of stress is established, the expression for interface friction assuming Coulomb's law is derived. The analytical model is verified by a comparison with finite element results. Finally, the potential applications of the developed analytical model are discussed.

3 Stress and Strain Analysis of the Guiding Zone Tribotest

3.1 Assumptions. The loading conditions in the guiding zone where the material is fed toward the die cavity are dictated by the internal pressure and axial feeding. The axial feeding is generally done at a relatively lower fluid pressure as compared with the calibration pressure, which is activated at the end of the THF process. The loading process in the guiding zone can be considered to be approximately proportional along the tube length. Thus, Hencky's deformation theory can be applied in the analysis. It has been shown that under proportional loading, the magnitudes of resulting strains are path independent and reduce the governing equations to Hencky's total deformation theory [17]. Researchers have also shown that the deformation theory of plasticity may be used for a range of loading paths other than the proportion loading without violating the general requirements for physical soundness of plasticity theory [18,19].

Varma et al. [20] found that by changing the loading conditions during hydroforming, one can subject the tube to nonproportional or proportional strain paths. In their studies, they found that non-

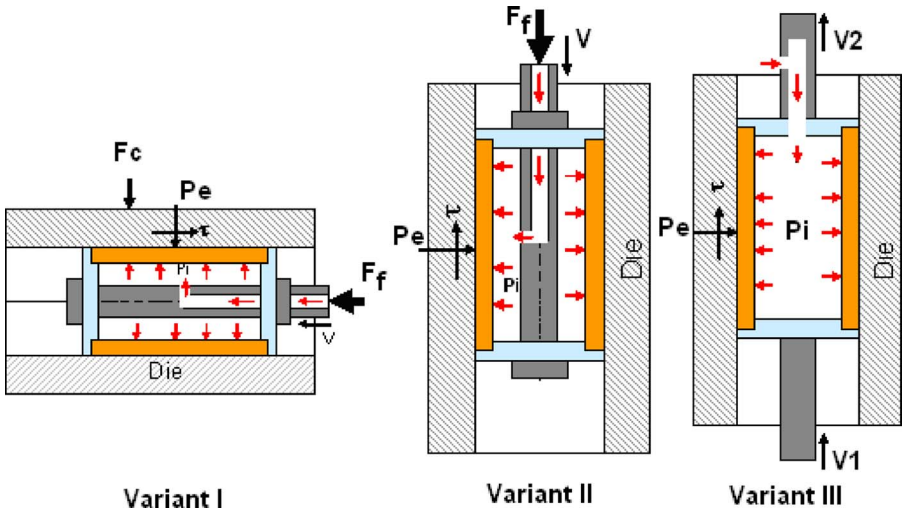

Fig. 2 Variants of guiding zone tribotests

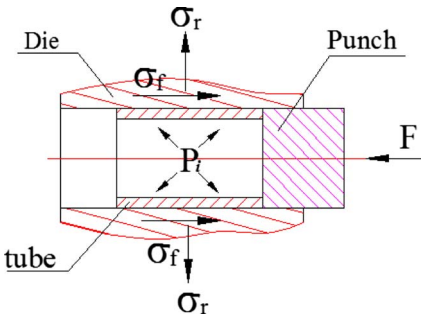

Fig. 3 Scheme of guiding zone tribotest

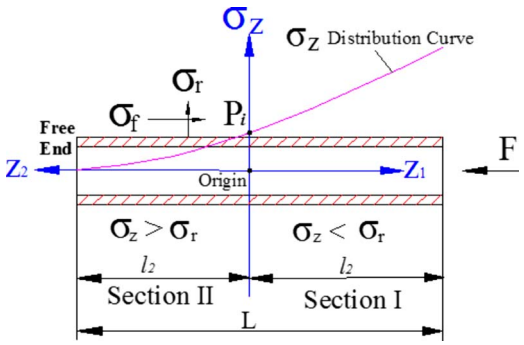

Fig. 5 Stress state of tube covered by sections I and II

proportional conditions occurs when fluid pressure along with axial end feed is prescribed, whereas the proportional condition is observed when the fluid volume flow rate is specified in conjunction with axial contraction. In this study, Hencky's deformation theory is adopted. Various simplifications and assumptions used throughout the derivations are as follows.

- The tube is considered as a thin wall structure.
- Longitudinal stress through the thickness direction is assumed to be uniform.
- Shear stress through the thickness direction induced by friction force is neglected.
- Tubular material is assumed to be isotropic.
- Throughout the process. the material is considered to be in plastic state of deformation.

3.2 Stress Analysis. The scheme of the test is shown in Fig. 3. Figure 4 shows the stress state on the element cut from the tube wall. In the guiding zone tribotest, the tube is first pressurized. When the yielding pressure is attained, the tube expands until it establishes contact with the die. The gap between the die and the tube before pressurization starts is of the order of 1% of the tube diameter.

Since the tube is pushed against a frictional surface, the internal pressure P_i has forced the tube material to conform to the die surface such that strain in the hoop direction $\varepsilon_\theta=0$, achieving plane strain condition. Based on Hencky's total deformation theory [17] and the condition $\varepsilon_\theta=0$, Eq. (4) holds.

$$\varepsilon_\theta = \frac{d\bar{\varepsilon}}{d\bar{\sigma}}\,(\sigma_\theta - (\sigma_Z + \sigma_r)/2)) = 0 \Rightarrow \sigma_\theta = (\sigma_Z + \sigma_r)/2 \tag{4}$$

Taking the balance of forces in the r-θ and r-z plane, where the element width is 1 unit, Eqs. (5) and (6) can be obtained.

$$\left.\begin{aligned} P_i r_i \theta + \sigma_r r_0 \theta - 2\sigma_\theta t \sin\frac{\theta}{2} = 0 \\ \lim_{\theta\to 0} \sin\left(\frac{\theta}{2}\right) = \frac{\theta}{2} \end{aligned}\right\} \Rightarrow \sigma_\theta = (\sigma_r r_o + P_i r_i)/t \tag{5}$$

$$(\sigma_Z + d\sigma_Z)2\pi r_o(t+dt) - \sigma_Z(z)2\pi r_o t + \sigma_f 2\pi r_o dz = 0 \tag{6}$$

In the guiding zone tribotest, radial stress is compressive stress, i.e., $\sigma_r<0$; thus the friction law can be expressed as

$$\sigma_f = \mu|\sigma_r| = -\mu\sigma_r$$

$$\left.\begin{aligned} \frac{d\sigma_Z}{dz} = \frac{\mu}{t}\sigma_r - \frac{\sigma_Z}{dz}\frac{dt}{t} \\ \frac{dt}{t} = d\varepsilon_r = -d\varepsilon_Z \end{aligned}\right\} \Rightarrow \frac{d\sigma_Z}{dz} = \frac{\mu}{t}\sigma_r + \sigma_Z\frac{d\varepsilon_z}{dz} \tag{7}$$

In the guiding zone tribotest, there are two sections along the longitudinal direction of the tube (Fig. 5).

(a) *Section I*: The section near the tube end which is pushed a by punch and characterized by the conditions that $\sigma_z<\sigma_r$ and $\varepsilon_z<0$.

(a) *Section II*: The section near the free tube end characterized by the conditions that $\sigma_r<\sigma_z$ and $\varepsilon_z>0$.

In other words, section I will exhibit compressive longitudinal stress while section II will exhibit tensile longitudinal stress. It should be noted that the lengths l_1 and l_2 will vary based on the location along the tube where $\sigma_r=\sigma_z$ Details on the determination of l_1 and l_2 are given in Sec. 3.4. Using Von Misses yield criteria, the effective stress and strain under plane strain condition, $\varepsilon_\theta=0$, can be expressed by Eqs. (8) and (9) for sections I and II, respec-

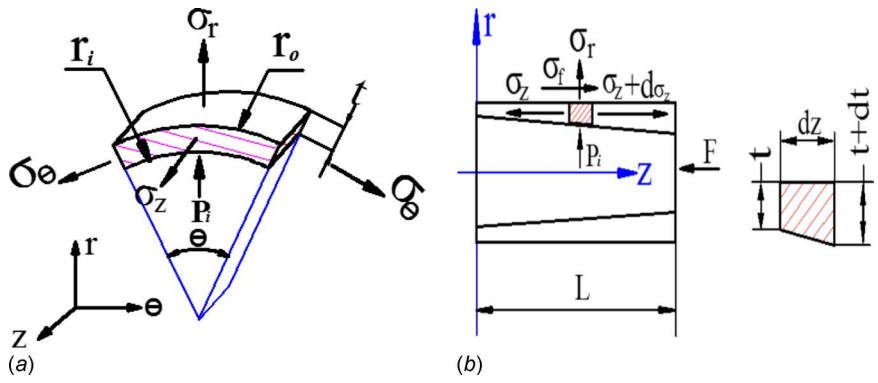

Fig. 4 Stresses acting on the element: (*a*) *r*-θ plane and (*b*) *r*-*z* plane

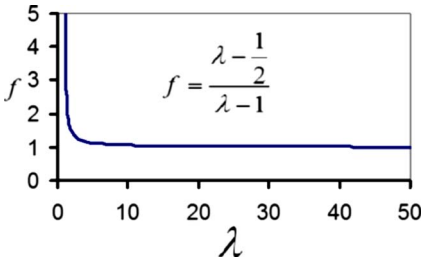

Fig. 6 Relationship between *f* and λ

tively. Flow stress of most metals used in metal forming closely obey the power $\bar{\sigma}=K\bar{\varepsilon}^n$. Substituting power law into Eqs. (8) and (9) leads to Eq. (10).

$$\bar{\sigma}=\frac{1}{\beta}(\sigma_r-\sigma_Z),\quad \bar{\varepsilon}=-\beta\varepsilon_z,\quad \beta=\frac{2}{\sqrt{3}} \tag{8}$$

$$\bar{\sigma}=\frac{1}{\beta}(\sigma_Z-\sigma_r),\quad \bar{\varepsilon}=\beta\varepsilon_z,\quad \beta=\frac{2}{\sqrt{3}} \tag{9}$$

$$\sigma_r-\sigma_Z=K\beta^{n+1}\varepsilon_z^n \quad \text{section I}$$

$$\sigma_Z-\sigma_r=K\beta^{n+1}\varepsilon_z^n \quad \text{section II} \tag{10}$$

Equations (4), (5), (7), and (10) give the inter-relationship of stresses along the tube length. To have a complete description of the state of stress along the tube, the longitudinal strain ε_z needs to be determined. Also, hoop stress and longitudinal stress need to be expressed in terms of interface friction and other known quantities.

3.3 Derivation of Strain. The longitudinal strain ε_z in section I will be derived from Eqs. (4), (5), (7), and (10). The tube length of section I is set to l_1 and the location of σ_z equal to σ_r is set as the original point of the z-axis, which lead to the boundary conditions $\varepsilon_z=0$ at $z=0$. The radial stress and longitudinal stress given in Eqs. (11) and (12) are obtained by combining Eqs. (4), (5), and (10). Substituting the radius to thickness ratio, λ, and f as a function of λ into Eq. (12), Eq. (13) can be obtained.

$$\sigma_r=-\frac{K\beta^{n+1}(-\varepsilon_z)^n+P_i\frac{2r_i}{t}}{\frac{2r_o}{t}-2} \tag{11}$$

$$\sigma_z=-\frac{\left(\frac{r_o}{t}-\frac{1}{2}\right)K\beta^{n+1}(-\varepsilon_z)^n+P_i\frac{r_i}{t}}{\frac{r_o}{t}-1} \tag{12}$$

$$\sigma_z=-(fK\beta^{n+1}(-\varepsilon_z)^n+P_i) \tag{13}$$

where $r_i/t=(r_o-t)/t$, $\lambda=r_o/t$, and $f=\left(\lambda-\frac{1}{2}\right)/(\lambda-1)$.

As the tube is pushed through the die, the variable t (thickness of tube) varies along the z-axis during deformation. Figure 6 shows the change in parameter f with respect to λ. It can be observed that when $\lambda=5$, and $f=1.125$. As λ increases beyond 5, f decreases asymptotically to 1. Thus for values of λ greater than 5, the variation in parameter f can be ignored. Thus, f can be taken as a constant in the longitudinal direction.

Equation (14) is obtained by taking a derivative of σ_z pertaining to Eq. (13) with respect to dz. Substituting Eqs. (7), (11), and (12) into Eq. (14), Eq. (15) can be obtained. With axial load, the tube thickness t will increase and can be computed as $t=t_0e^{-\varepsilon z}$ from volume constant condition. Substituting thickness expression into Eq. (15) and integrating it, Eq. (16) can be obtained.

$$\frac{d\sigma_z}{dz}=-\frac{d(fK\beta^{n+1}(-\varepsilon_z)^n+P_i)}{dz}=\frac{\frac{r_o}{t}-\frac{1}{2}}{\frac{r_o}{t}-1}K\beta^{n+1}n(-\varepsilon_z)^{n-1}\frac{d\varepsilon_z}{dz} \tag{14}$$

$$\left(\frac{r_o}{t}-\frac{1}{2}\right)K\beta^{n+1}n(-\varepsilon_z)^{n-1}\frac{d\varepsilon_z}{dz}=-\left\{\frac{\mu}{2t}K\beta^{n+1}(-\varepsilon_z)^n+P_i\frac{\mu}{t}\frac{r_i}{t}\right\}-\left\{\left(\frac{r_o}{t}-\frac{1}{2}\right)K\beta^{n+1}(-\varepsilon_z)^n+P_i\frac{r_i}{t}\right\}\frac{d\varepsilon_z}{dz} \tag{15}$$

$$\int_0^{\varepsilon_z}-\frac{\left(\frac{r_o}{t_0e^{-\varepsilon_z}}-\frac{1}{2}\right)K\beta^{n+1}\{n(-\varepsilon_z)^{n-1}+(-\varepsilon_z)^n\}+P_i\frac{r_i}{t_0e^{-\varepsilon_z}}}{\frac{\mu}{2t_0e^{-\varepsilon_z}}K\beta^{n+1}(-\varepsilon_z)^n+P_i\frac{\mu r_i}{(t_0e^{-\varepsilon_z})^2}}d\varepsilon_z=z \tag{16}$$

Equation (16) can be solved numerically to obtain longitudinal strain, ε_z, which can be substituted into Eqs. (11) and (12) to compute longitudinal stress, σ_z, and radial stress, σ_r, respectively. When longitudinal strain ε_z is small, it is reasonable to assume that the deformed tube thickness t approximate the original thickness t_0. Thus, Eq. (7) can be reduced to $d\sigma_Z/dz=(\mu/t)\sigma_r$. Thus the second term on the left hand side of Eq. (15) can be ignored. By substituting $r_o/t_o=\alpha$ and $r_i/t_o=\alpha-1$ into Eq. (15), Eq. (17) can be obtained. Integrating Eq. (17), and considering the boundary conditions that $\varepsilon_z=0$ at $z=0$, an explicit expression for ε_z can be obtained as given in Eq. (18). Details on the integration of Eq. (17) are given in Appendix C.

$$\int_0^{\varepsilon_z}-\frac{\left(\alpha-\frac{1}{2}\right)K\beta^{n+1}n(-\varepsilon_z)^{n-1}}{\frac{\mu}{2t_0}K\beta^{n+1}(-\varepsilon_z)^n+P_i\frac{\mu(\alpha-1)}{t_0}}d\varepsilon_z=z \tag{17}$$

$$\varepsilon_z=-\left\{\frac{2(\alpha-1)}{K\beta^{n+1}}p_i\left(\exp\frac{\mu z}{(2\alpha-1)t_0}-1\right)\right\}^{1/n} \tag{18}$$

By substituting Eq. (18) into Eqs. (11) and (12), the radial and longitudinal stresses can be obtained as functions of interface friction, internal pressure, wall thickness, and ratio of tube outer radius to tube wall thickness. Equation (19) gives a complete description of the stresses and strains of section I.

$$\sigma_r=-\left\{p_i\exp\frac{\mu z}{(2\alpha-1)t_0}\right\}$$

$$\sigma_z=-\left\{(2\alpha-1)\left(\exp\frac{\mu z}{(2\alpha-1)t_0}-1\right)p_i+p_i\right\}$$

$$\sigma_\theta=-\left\{\frac{(2\alpha-1)}{2}\left(\exp\frac{\mu z}{(2\alpha-1)t_0}-1\right)p_i+\frac{1}{2}\left(\exp\frac{\mu z}{(2\alpha-1)t_0}+1\right)p_i\right\}$$

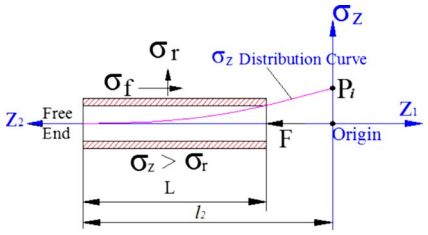

Fig. 7 Stress state of tube fully covered by section II

$$\varepsilon_z = -\left\{\frac{2(\alpha-1)}{K\beta^{n+1}} p_i\left(\exp\frac{\mu z}{(2\alpha-1)t_0} - 1\right)\right\}^{1/n}, \quad \varepsilon_r = -\varepsilon_z, \quad \varepsilon_\theta = 0 \tag{19}$$

By the same derivation process, Eq. (20) can be obtained to describe the stresses and strains of section II. The detailed derivation of Eq. (20) is given in Appendix A.

$$\sigma_r = -\left\{p_i \exp\frac{-\mu z}{(2\alpha-1)t_0}\right\}$$

$$\sigma_z = -\left\{p_i - p_i(2\alpha-1)\left(1-\exp\frac{-\mu z}{(2\alpha-1)t_0}\right)\right\}$$

$$\sigma_\theta = -\left\{\frac{1}{2}p_i\left(1+\exp\frac{-\mu z}{(2\alpha-1)t_0}\right) + \frac{1}{2}(2\alpha-1)\left(1-\exp\frac{-\mu z}{(2\alpha-1)t_0}\right)p_i\right\}$$

$$\varepsilon_z = \left\{\frac{2(\alpha-1)}{K\beta^{n+1}} p_i\left(1-\exp\frac{-\mu z}{(2\alpha-1)t_0}\right)\right\}^{1/n}, \quad \varepsilon_r = -\varepsilon_z, \quad \varepsilon_\theta = 0 \tag{20}$$

3.4 Determination of Deformed Length L, and Lengths l_1 and l_2 for Sections I and II

3.4.1 Determination of Deformed Length L When the Tube is Fully Covered by Section II. In order to determine whether the tube is fully covered by section II, the boundary conditions are first examined. The boundary condition of this tribotest is such that one end of the tube is free, for which σ_z is zero. This meets the conditions of section II that $\sigma_z > \sigma_r$. Substituting $\sigma_z = 0$ into Eq. (20) l_2 can be determined.

$$p_i - p_i(2\alpha-1)\left(1-\exp\frac{-\mu l_2}{(2\alpha-1)t_0}\right) = 0$$

$$\Rightarrow l_2 = \frac{(2\alpha-1)t_0}{\mu}\ln\left(\frac{2\alpha-1}{2\alpha-2}\right) \tag{21}$$

From Eq. (21), it can be seen that when μ is very small, l_2 can theoretically be greater than L. Therefore, when $\frac{1}{\mu}(2\alpha-1)t_0 \ln((2\alpha-1)/(2\alpha-2)) \geq L$, the tube is fully covered by section II, as shown in Fig. 7. Since this condition occurs under lower friction, the change in tube length due to deformation is insignificant. Thus the final tube length, L, can be approximated to the original tube length L_0. Alternatively, we can determine, L, by volume constancy condition, as given in Eq. (22).

$$V_0 = V \Rightarrow 2\pi r_o L_0 t_0 = 2\pi r_o \int_0^L t_0 e^{\varepsilon_r} dz \tag{22}$$

$$L_0 = \int_0^L e^{\varepsilon_r} dz, \quad l_2 = L, \quad l_1 = 0 \tag{23}$$

where V_o is the original volume of the tube and V is the volume of the tube after test.

Because the tube is fully covered by section II, only Eq. (20) is used to calculate the stress and strain. L can be calculated from Eq. (23), where ε_r is taken from Eq. (20). Thus, when the tube is fully covered by section II, the deformed length L, and lengths l_1 and l_2 for sections I and II, respectively, can be determined by Eq. (23).

3.4.2 Determination of l_1 and l_2 When the Tube is Covered by Sections I and II. The state of stress when the tube is covered by sections I and II is shown in Fig. 5. The length, L, is calculated by volume constancy using Eq. (22), where the volume of the tube is calculated by summing the respective volumes for sections I and II, respectively, as shown in Eq. (24). l_1 and l_2 are finally determined by Eq. (25).

$$L_0 = \int_0^{L-\frac{1}{\mu}(2\alpha-1)t_0 \ln((2\alpha-1)/(2\alpha-2))} \exp(-\varepsilon_Z) dz_2 + \int_0^{\frac{1}{\mu}(2\alpha-1)t_0 \ln((2\alpha-1)/(2\alpha-2))} \exp(-\varepsilon_Z) dz_2 \tag{24}$$

$$l_2 = \frac{(2\alpha-1)t_0}{\mu}\ln\left(\frac{2\alpha-1}{2\alpha-2}\right), \quad l_1 = L - l_2 \tag{25}$$

4 Derivation of Expression for Friction Coefficient

As discussed in Sec. 1, most of the existing tribotest variants for the guiding zone assume that the interface pressure between the tube and the die is approximately the same as the internal tube fluid pressure [16,21]. The radial stress derived in Sec. 3 (Eqs. (19) and (20)) shows clearly that the interface pressure may vary drastically depending on the coefficient of friction and other geometric variables. In this section, we will derive the expression for interface friction. This derivation will include parameters that can be obtained in the guiding zone tribotest experiments, such as friction force (F_f) measured by the load cell (refer to Fig. 2) and fluid pressure (Pi) supplied inside the tube, and the measured original tube length (L_o) and deformed tube length (L).

In most of the guiding zone tribotest, the longitudinal strain is small and the radial pressures can be determined by Eqs. (19) and (20), which give the contact pressures at the tool-tube interface. The two equations represent two contact scenarios that may occur during the test. One of the contact conditions is that the tube is full covered by section II, and the other is that the tube is covered by sections I and II. When the tube is covered by sections I and II, Eqs. (19) and (20) are both used to calculate the contact pressure. The state of stress under this condition is shown in Fig. 5. Friction force F_f is now expressed by Eq. (26). Equation (27) is obtained by substituting Eqs. (19) and (20) into Eq. (26). Substituting Eq. (25) into Eq. (28), Eq. (29) is obtained. From Eq. (29), the coefficient of friction μ can be expressed as shown in Eq. (30).

$$F_f = \int_0^{l_2} 2\pi r_o \mu |\sigma_r| dz_2 + \int_0^{l_1} 2\pi r_o \mu |\sigma_r| dz_1 \tag{26}$$

$$F_f = \int_0^{l_2} 2\pi r_o \mu p_i \exp\left(\frac{-\mu z_2}{(2\alpha-1)t_0}\right) dz_2 + \int_0^{l_1} 2\pi r_o \mu p_i \left(\frac{\mu z_1}{(2\alpha-1)t_0}\right) dz_1 \tag{27}$$

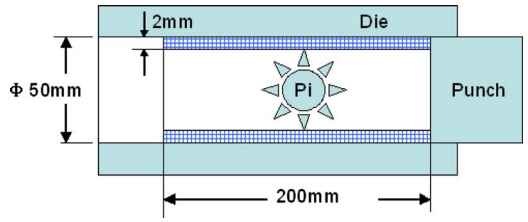

Fig. 8 Schematic of FEA model for the guiding zone test

$$F_f = 2\pi r_o(2\alpha - 1)t_0 p_i\left(\exp\frac{\mu l_1}{(2\alpha-1)t_0} - \exp\frac{-\mu l_2}{(2\alpha-1)t_0}\right) \quad (28)$$

$$F_f = 4\pi r_o(\alpha - 1)t_0 p_i\left(\exp\frac{\mu L}{(2\alpha-1)t_0} - 1\right) \quad (29)$$

$$\mu = \frac{(2\alpha-1)t_0}{L}\ln\left(\frac{F_f}{4\pi r_o p_i(\alpha-1)t_0} + 1\right) \quad (30)$$

It should be noted that the derivation that lead to Eq. (30) focused on expressing Coulomb friction as a function of interface pressure and friction stress. During the experiment the frictional force, F_f, can be measured. Since the normal load cannot easily be measured, the analytical model provides the normal stress, σ_r. The influence of tube surface roughness and speed of the punch is not considered.

5 Results and Discussion

5.1 Comparison Between Analytical Model and Finite Element Simulation Results. Finite element simulations for the guiding zone were carried out in order to validate the closed-form solutions developed for contact pressure, longitudinal stress, effective stress and strain, longitudinal strain, given in Eqs. (11), (12), (16), and (20), and the solutions for friction force given in Eq. (26). The finite element simulations were carried out by commercial rigid plastic implicit finite element analysis (FEA) code, DEFORM 2D. Various case studies were simulated, two of which are presented in this paper. Figure 8 shows the FEA model used. The die and punch were treated as rigid bodies and the tube was discretized by 2000 quadrilateral elements with five elements across the wall thickness. The power law flow stress equation was used with strength coefficient $K=500$ MPa and strain hardening exponent $n=0.3$. The forming duration was set at 10 s. The die was fixed while the punch was assigned a longitudinal velocity of 15 mm/s. A pressure of 30 MPa was applied on the inner surface of the tube as internal fluid pressure. The interface friction at the die-tube interface was prescribed by assuming Coulombs friction law.

Figure 9 presents state variables with two friction condition: one for friction coefficient of $\mu=0.05$ and another for $\mu=0.2$. Figure 9 shows the comparison between the analytical model and the FEA model for contact pressure, effective stress, and effective strain distribution. The analytical model agrees well with the FEA results for both friction conditions. Figure 9(*f*) show the punch load prediction comparison for $\mu=0.05$ and $\mu=0.2$. The punch load for $\mu=0.05$ from analytical model is 50 kN. When friction coefficient of $\mu=0.2$ was used, the load increased to 240 kN. The corresponding FEA results for the punch load are 44 kN and 210 kN for $\mu=0.05$ and $\mu=0.2$, respectively. These values are close to that obtained using the analytical model.

The punch load history from the finite element simulation shown in Fig. 9(*f*) shows two distinct stages. The punch load increases gradually with an increase in the forming time up to a maximum load; thereafter a constant load is maintained for the whole forming duration. The initial stage shows load buildup before the tube starts to slide against the die. The analytical model provides punch load at the commencement of sliding, i.e., the initial stage is not accounted in this model. It should also be noted that the load built-up duration before the tube start to slide depends on the prescribed interface friction, as can be observed in Fig. 9(*f*).

5.2 Potential Areas of Application for the Established Closed-Form Solutions. The established equations can provide local distribution of field variables along the tube length in terms of principal stresses and strains as a function of friction coefficient, fluid pressure, and geometric variables. These equations can facilitate better understanding of tribological aspects in the guiding zone and can be helpful in the design of tooling for THF.

Tribological aspects in THF. Most frictional data obtained from existing tribotests for the guiding zone have been determined by assuming that the internal fluid pressure is the same as the interface pressure. Figures 9(*a*) show that the interface pressure can increase dramatically beyond the internal fluid pressure (P_i). Figure 9(*a*) shows that at a friction coefficient of $\mu=0.2$, the interface pressure varied from 30 MPa to 62 MPa when the internal fluid pressure was 30 MPa. While coefficient of friction may be reasonably approximated by assuming that internal fluid pressure equals interface pressure, using the internal pressure for studying other tribological aspects such as die wear may lead to significant error. Figure 9(*c*) shows the steep gradients for the longitudinal stress of the order of 0–500 MPa. High compressive stresses dictated by σ_z can provide useful information on how certain lubricants may perform, as well as giving insight on possible changes in the tube surface morphology. Furthermore, knowing the contact stress at the tool-tube interface together with longitudinal stress distributions should provide information to the tribologist/lubricant formulator on whether microplastohydrodynamic or microplastohydrostatic lubrication mechanisms are likely to occur. For highly strain hardening materials, the local strain distribution may provide insight as to what types of lubricant chemistries may be applicable on surfaces that exhibit significant hardening during deformation.

As discussed in Sec. 1, most of the guiding zone tribotests developed to date assume that the interface pressure to be equal to the internal fluid pressure. From the derived equations for contact pressure, see Fig. 9(*a*), the approximation of internal pressure will be reasonable only when the friction level is small and when the tube sample is shorter. As seen in Fig. 9(*a*), up to a tube length of 75 mm, the contact pressure is equal to the internal fluid pressure when $\mu=0.05$. The experimental results for the guiding zone from Hwang et al. [21] were compared with the results from the derived analytical model. Hwang et al. [21] carried out the experiments using 70 mm long tube with an outer diameter of 72 mm and a wall thickness of 3 mm. The internal pressure of 20 MPa was assumed to be equal to the contact pressure. Using lubricant R68, they obtained a friction load of 14.5 kN, which yielded a friction coefficient $\mu=0.046$. From the expression given in Eq. (30), where $\alpha=r_o/t_o=12$, the interface friction can be determined as follows:

$$\mu = \left(\frac{2\times 12-1}{70}\right)3\ln\left(\frac{14{,}500}{4\pi\times 36\times 20(12-1)3}+1\right) = 0.0467$$

The friction value obtained from the analytical expression is almost identical to what was obtained by Hwang et al. [21]. As discussed above this should be the case with low friction levels.

Tube hydroforming tooling design. The guiding zone is an integral part of THF tooling. The purpose of the guiding zone is to hold and align the tube. It is where the tube is completely sealed so that high forming pressure can be attained. The guiding zone also serves as a gateway for the material to be fed to the die cavity. Since the highest sliding velocity is encountered in this zone, the die is susceptible to failure due to wear. Figure 1(*b*) shows a typical THF tooling with feeding die inserts at the guiding zone. Due to high sliding velocity and friction stress, the guid-

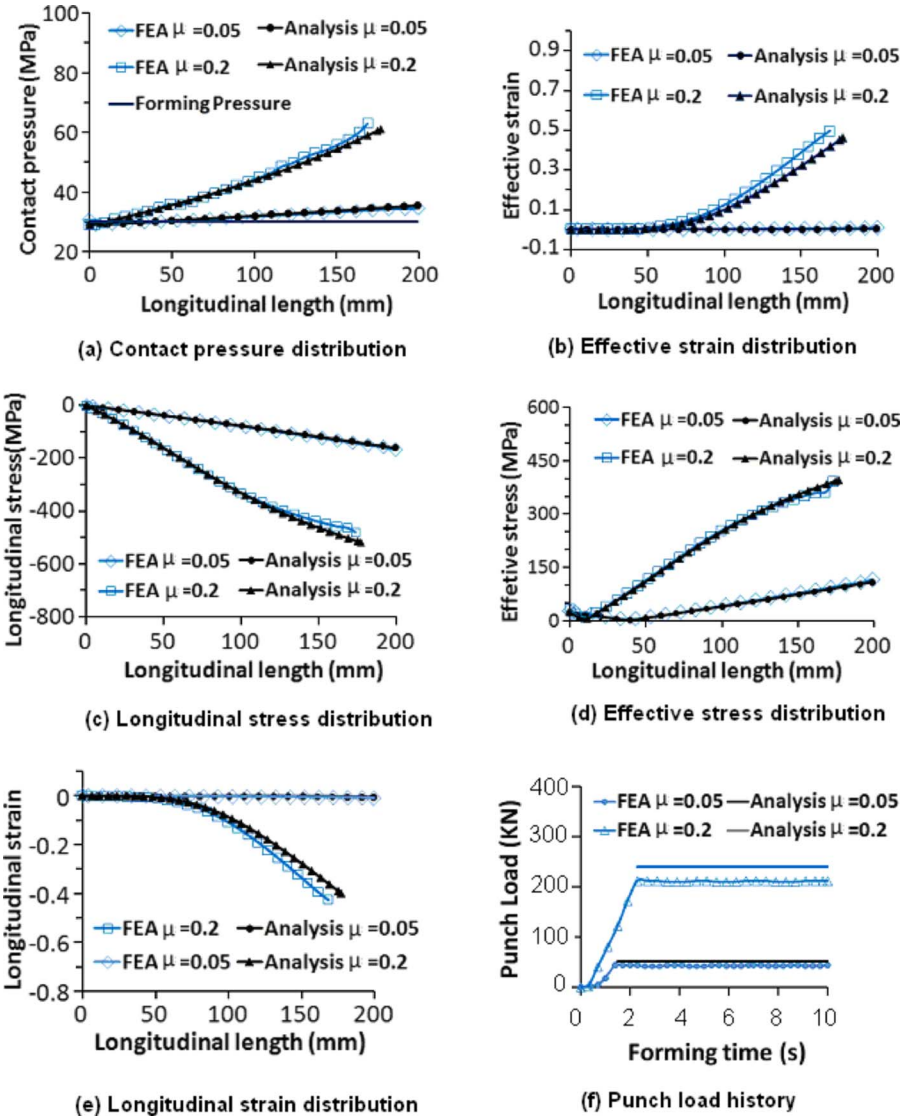

Fig. 9 Influence of interface friction on contact pressure, effective stress, and effective strain distribution

ing zone may be subjected to severe wear. Using the established equations, tool designers can quickly plot a "friction hill envelope" to aid in determining suitable geometric parameters, load requirements for press and axial cylinder actuators, etc. From Eq. (30), we saw that the contact pressure is formulated based on the coordinate system CS1 depicted again in Fig. 10 where the origin at the centerline point meets the condition ($\sigma_z = \sigma_r$).

If a new coordinate system CS2 (Fig. 10) is established at the free end of the tube, then point P1 in section I has two sets of coordinate (z_1, r) and (z, r) for CS1 and CS2, respectively, while point P2 in the section II has two sets of coordinate (z_2, r) and (z, r) for CS1 and CS2, respectively. By the geometrical relation, Eq. (31) can be obtained. Combining Eqs. (19) and (20) lead to Eq. (32).

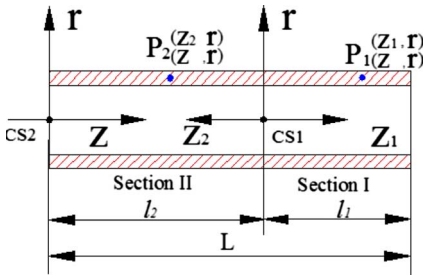

Fig. 10 Coordinate systems of tube

$$\left.\begin{aligned} Z &= Z_1 + L_2 \\ L_2 &= Z_2 + Z \end{aligned}\right\} \Rightarrow \begin{cases} Z_1 = Z - L_2 \\ Z_2 = L_2 - Z \end{cases} \tag{31}$$

$$\sigma_r = -p_i \exp\frac{\mu z_1}{(2\alpha - 1)t_0}, \quad 0 \le z_1 \le l_1$$

$$\sigma_r = -p_i \exp\frac{-\mu z_2}{(2\alpha - 1)t_0}, \quad 0 \le z_2 \le l_2 \tag{32}$$

Substituting Eq. (31) into Eq. (32), Eq. (33) is obtained, which can be simplified to Eq. (34). By substituting Eq. (25) into Eq. (34), the contact pressure in the form given in Eq. (35) is obtained.

$$\sigma_r = -p_i \exp\frac{\mu(Z - L_2)}{(2\alpha - 1)t_0}, \quad L_2 \le z \le L$$

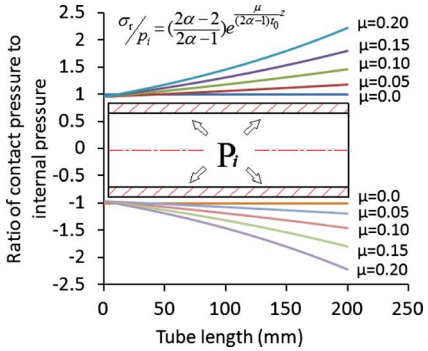

Fig. 11 Friction hill envelope for THF guiding zone

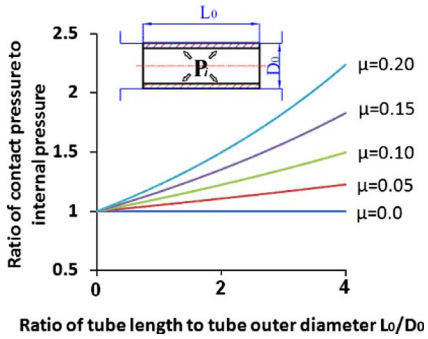

Fig. 12 Variation of maximum R_p with L_o/D_o ratio for various friction conditions

$$\sigma_r = -p_i \exp\frac{\mu(Z-L_2)}{(2\alpha-1)t_0}, \quad 0 \le z \le L_2 \tag{33}$$

$$\sigma_r = -p_i \exp\frac{\mu(Z-L_2)}{t_0(2\alpha-1)} \tag{34}$$

$$\sigma_r = -p_i \exp\left(\frac{\mu}{(2\alpha-1)t_0}\left(Z - \frac{(2\alpha-1)t_0}{\mu}\ln\frac{2\alpha-1}{2\alpha-2}\right)\right)$$

$$= -\left(\frac{2\alpha-2}{2\alpha-1}\right)p_i \exp\frac{\mu z}{(2\alpha-1)t_0} \tag{35}$$

Equation (35) can be used to plot a friction hill envelope for the guiding zone. Figure 11 shows an example of a friction hill envelope for a guiding zone with 200 mm tube length, 50 mm tube diameter, and 2 mm wall thickness at an internal pressure P_i. As seen in Fig. 11, when $\mu=0.2$, the maximum pressure acting on the tube-die interface is over two times higher than the fluid pressure.

A more generic form, however, is a dimensionless scheme that shows the variation in maximum die contact pressure to fluid pressure ratio (σ_r/P_i) with tube length to diameter ratio (L_o/D_o) for various friction conditions. The variable R_p is defined as ratio of contact pressure, σ_r, to internal pressure, P_i. By considering the tube as a thin wall structure where $\alpha > 10$, the ratio R_p can be expressed as a function of interface friction and geometric variables. From Eq. (36), it can be seen that the maximum R_p occurs at the loaded end of the tube where $Z=L_o$, as expressed in Eq. (37).

$$R_p = \left|\frac{\sigma_r}{p_i}\right| = \left(\frac{2\alpha-2}{2\alpha-1}\right)\exp\frac{\mu z}{(2\alpha-1)t_0} \approx \exp\frac{\mu z}{D_o} \tag{36}$$

where

$$\left(\frac{2\alpha-2}{2\alpha-1}\right) \approx 1, \quad (2\alpha-1)t_0 = \left(2\frac{r_o}{t}-1\right)t_0 \approx D_o$$

$$\text{Max}(R_p) \approx \exp\frac{\mu L_o}{D_o} \tag{37}$$

Equation (37) shows that the maximum contact pressure along the tube length depends on the friction coefficient μ and the ratio of tube length L_o to the tube outer diameter D_o. Figure 12 shows the variation in R_p with the L_o/D_o ratio. It can be seen that maximum contact pressure increases rapidly with the increase in L_o/D_o ratio. Thus, the ratio, L_o/D_o, is a critical parameter in the design of the guiding zone for tube hydroforming systems.

The friction hill envelope given in Fig. 11 and variation in Max R_p versus L_o/D_o given in Fig. 12 have been established based on Eq. (35), which is valid for low strain range. Figures 11 and 12 can therefore be applied when the tube length to diameter ratio L_o/D_o does not exceed 4 and a maximum coefficient of friction of $\mu=0.2$. Appendix B gives details on derivation of expressions for determining state variables at higher strain level ($\varepsilon_z=0.1-2.0$). An example of tube-die contact pressure distribution at higher strain level is given in Fig. 13. These curves were generated by the derived expression given in Appendix B. Figure 13 shows the maximum pressure that can be generated when an internal pressure of 60 MPa is applied on a tubular material with a strain hardening exponent, $n=0.3$, and a strength coefficient, $K=500$ MPa.

As can be seen from Fig. 13, an original tube length of 500 mm ($L_o/D_o=10$) result in a contact pressure of up to 450 MPa when a coefficient of friction of $\mu=0.4$ is exhibited at the interface. This pressure is over seven times higher than the forming pressure. The figure also shows that the increase in interface pressure is highly influenced by the increase in L_o/D_o ratio. Figure 13 also shows the comparison between the analytical model and FEA for tube lengths of 200 mm and 400 mm. With 200 mm tubing, FEA shows contact pressure at the tube-die interface of 86 MPa, 113 MPa, and 138 MPa for $\mu=0.1$, $\mu=0.2$, and $\mu=0.3$, respectively, whereas the analytical model exhibited contact pressures of 87 MPa, 109 MPa, and 133 MPa for $\mu=0.1$, $\mu=0.2$, and $\mu=0.3$ respectively. As the tube is pushed in the guiding zone, tube thickening will occur and the tube length will be shortened. For an initial tube length of 200 mm, FEA shows that final deformed tube lengths were 181 mm, 147 mm, and 127 mm for $\mu=0.1$, $\mu=0.2$, and $\mu=0.3$, respectively. The analytical model resulted in final tube lengths of 181 mm, 150 mm, and 130 mm for $\mu=0.1$, $\mu=0.2$, and $\mu=0.3$, respectively. Good agreement can be observed between analytical model and FEA results.

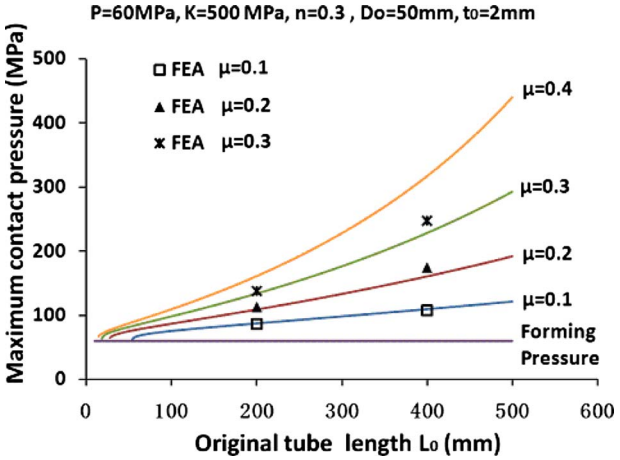

Fig. 13 Evolution of friction hill envelop and maximum contact pressure for a tubular material with $K=500$ MPa, $n=0.3$, and a forming pressure of 60 MPa

6 Conclusions

Closed-form solutions that characterize the guiding zone tribotest for tube hydroforming were established based on a mechanistic approach. From the derived analytical model field, variables can be computed along the tube. These variables include (a) contact pressure distribution, (b) effective stress and strain distribution, (c) longitudinal stress and strain distribution, and (d) hoop stress distribution.

Based on the derived equation for the contact pressure at the tool-tube interface, an expression for determining the coefficient of friction for the guiding zone tribotest was established. This expression is a function of tube geometric variables, internal pressure, and friction force obtained from tribotest experiment.

Through this study, friction hill envelopes for the guiding zone were established. These friction hill envelopes show the variation in contact pressure along the tube length as a function of friction coefficient. The study has also shown that the maximum contact pressure at the tool-tube interface increase rapidly with the increase in L_o/D_o ratio. Thus, the ratio L_o/D_o is a critical parameter in the design of the guiding zone for tube hydroforming systems.

Acknowledgment

The authors would like to acknowledge the National Science Foundation, through which this work was funded under Project No. DMI-0448885.

Nomenclature

μ = friction coefficient
F_f = friction force
F_c = normal load
F, F_1, F_2 = tube end load
P_i = internal pressure
Di = inner diameter
D_o = outer diameter
r_i = inner radius
r_o = outer radius
L = deformed tube length
L_o = initial tube length
l_1 = length of section I
l_2 = length of section II
t = deformed tube thickness
t_0 = original tube thickness
V = volume of deformed tube
V_0 = volume of initial tube
α = ratio of tuber outer radius to initial tube wall thickness
D_i = internal diameter of the tube
λ = ratio of tuber outer radius to instantaneous tube wall thickness
R_p = ratio of contact pressure to internal pressure
$\bar{\sigma}$ = effective stress
$\bar{\varepsilon}$ = effective strain
K = strength coefficient
n = strain hardening exponent
σ_z = longitudinal stress
σ_r = radial stress
σ_h = hoop stress
ε_z = longitudinal strain
ε_r = radial strain
ε_θ = hoop strain
Z, Z_1, Z_2 = longitudinal coordinate of the tube

Appendix A: Derivation of Strain ε_z in Section II of the Tube in the Guiding Zone

The longitudinal strain ε_z of section II can be derived from Eqs. (4), (5), (7), and (10). We set the tube length l_2 and the original point on the z-axis to where $\sigma_z=\sigma_r$ (refer Fig. 5). Because section II is near the free tube end, the longitudinal strain ε_z is small. Thus the term dt in Eq. (6) can be neglected and Eq. (6) can be reduced to Eq. (A1). The radial stress and longitudinal stress given in Eqs. (A2) and (A3) are obtained by combining Eqs. (4), (5), and (10). From Eq. (A3), Eq. (A4) can be derived. Substituting Eqs. (A1) and (A2) into Eq. (A4) yields Eq. (A5).

$$\frac{d\sigma_Z}{dz} = -\frac{\mu}{t}\sigma_r \tag{A1}$$

$$\sigma_r = -\frac{P_i\frac{2r_i}{t} - K\beta^{n+1}\varepsilon_z^n}{\frac{2r_o}{t} - 2} \tag{A2}$$

$$\sigma_z = -\frac{P_i\frac{r_i}{t} - \left(\frac{r_o}{t} - \frac{1}{2}\right)K\beta^{n+1}\varepsilon_z^n}{\frac{r_o}{t} - 1} \tag{A3}$$

$$\frac{d\sigma_z}{dz} = -\frac{\frac{r_o}{t} - \frac{1}{2}}{\frac{r_o}{t} - 1}K\beta^{n+1}n\varepsilon_z^{n-1}\frac{d\varepsilon_z}{dz} \tag{A4}$$

$$\left(\frac{r_o}{t} - \frac{1}{2}\right)K\beta^{n+1}n\varepsilon_z^{n-1}\frac{d\varepsilon_z}{dz} = \frac{\mu}{t}\frac{r_i}{t}P_i - \frac{\mu}{2t}K\beta^{n+1}\varepsilon_z^n \tag{A5}$$

Section II is near the free tube end and the axial load from the punch drops significantly in this section, which results in small axial strain ε_z. Thus, it is reasonable to assume that the deformed tube thickness t approximate original length t_0. Let $r_o/t_o=\alpha$, $r_i/t_o=\alpha-1$, and substitute into Eq. (A5) to obtain Eq. (A6). Integrating Eq. (A6), and invoking the boundary conditions that $\varepsilon_z=0$ at $z=0$, an explicit expression for ε_z can be obtained as given in Eq. (A7). By substituting Eq. (A7) into Eqs. (A2) and (A3), the radial and longitudinal stress can be obtained as functions of interface friction, internal pressure, wall thickness, and the ratio of tube outer radius to tube wall thickness.

$$\left(\alpha - \frac{1}{2}\right)K\beta^{n+1}n\varepsilon_z^{n-1}\frac{d\varepsilon_z}{dz} = \frac{\mu}{t}P_i(\alpha-1) - \frac{\mu}{2t}K\beta^{n+1}\varepsilon_z^n \tag{A6}$$

$$\varepsilon_z = \left\{\frac{2(\alpha-1)}{K\beta^{n+1}}p_i\left(1 - \exp\frac{-\mu z}{(2\alpha-1)t}\right)\right\}^{1/n} \tag{A7}$$

Appendix B: Explicit formula for Evaluation of State Variables at High Strain Range

Figure 14 shows a typical characteristic curve (Z versus ε_z) obtained from Eq. (16). Figure 14 shows that longitudinal strain ε_z varies approximately linearly with longitudinal tube length z at high strain range of ($\varepsilon_z=-0.1\sim\varepsilon_z=-2.0$). It is therefore possible to get an explicit formula for evaluating the state variables such as contact pressure at high strain level. From the linear relationship, Eq. (16) can be simplified to Eq. (B1).

$$z = z_{-0.1} + \mathrm{Slp}(\varepsilon_z + 0.1) \tag{B1}$$

where "Slp" is the slope of the curve and $Z_{-0.1}$ is the longitudinal length where the longitudinal strain is $\varepsilon_z=-0.1$. The slope of the curve can be computed approximately by substituting $\varepsilon_z=-1.0$ into the integrand at the left side of Eq. (16) which leads to Eq. (B2). $Z_{-0.1}$ can be obtained by substituting $\varepsilon_z=-1.0$ into Eq. (18), as shown in Eq. (B3). Note that the slope, Slp, is a function of K, n, r_o, t_o, Pi, and μ.

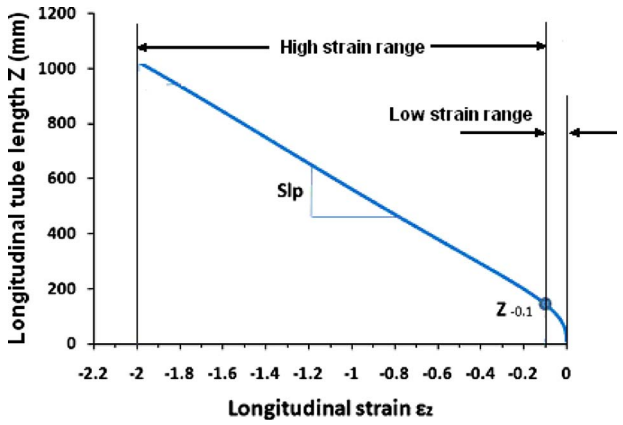

Fig. 14 Characteristic curve of Eq. (16)

$$\mathrm{Slp} = -\frac{\left(\frac{r_o}{t_0 e} - \frac{1}{2}\right)K\beta^{n+1}\{n+1\} + P_i\frac{r_o - t_0 e}{t_0 e}}{\frac{\mu}{2t_0 e}K\beta^{n+1} + P_i\frac{\mu r_i}{(t_0 e)^2}}$$

$$= -\frac{1}{\mu}\frac{(2\alpha - e)(n+1)K\beta^{n+1}t_0 e + 2P_i t_0 e(\alpha - e)}{eK\beta^{n+1} + 2P_i(\alpha - e)} - 0.1$$

$$= -\left\{\frac{2(\alpha-1)}{K\beta^{n+1}}p_i\left(e^{\frac{\mu}{(2\alpha-1)t_0}z_{-0.1}} - 1\right)\right\}^{1/n} \tag{B2}$$

$$z_{-0.1} = \frac{(2\alpha-1)t_0}{\mu}\ln\left(\frac{K\beta^{n+1}(0.1)^n}{2(\alpha-1)p_i} + 1\right) \tag{B3}$$

Substituting Eqs. (B2) and (B3) into Eq. (B1), an explicit expression for the longitudinal strain can be obtained, Eq. (B4). By substituting Eq. (B4) into Eqs. (11) and (12), the contact pressure and longitudinal stress can be expressed explicitly. The deformed tube length L can be evaluated by the volume constant condition as given in Eq. (B5). Substituting Eq. (B4) into Eq. (11), the explicit form for contact pressure evaluation is obtained as Eq. (B6). The expression for maximum pressure can be obtained by substituting $Z=L_o$ into Eq. (B6).

$$\varepsilon_z = -(0.1 + b\mu(z-c))$$

$$b = \frac{\{eK\beta^{n+1} + 2P_i(\alpha - e)\}}{(2\alpha - e)(n+1)K\beta^{n+1}t_0 e + 2P_i t_0 e(\alpha - e)}$$

$$c = \frac{(2\alpha-1)t_0}{\mu}\ln\left(\frac{K\beta^{n+1}(0.1)^n}{2(\alpha-1)p_i} + 1\right) \tag{B4}$$

$$V_0 = V \Rightarrow 2\pi r_0 t_0 L_0 = \int_0^L 2\pi r_0 t_0 \exp(0.1 + b\mu(z-c))dz$$

$$\Rightarrow L = \frac{\ln(\mu b L_0 + \exp(0.1 - \mu bc)) - 0.1}{b\mu} + c \tag{B5}$$

$$\sigma_r = -\frac{K\beta^{n+1}(0.1 + b\mu(z-c))^n t_0 e^{(0.1+b\mu(z-c))} + P_i 2(r_o - t_0 e^{(0.1+b\mu(z-c))})}{2(r_o - t_0 e^{(0.1+b\mu(z-c))})} \tag{B6}$$

Appendix C: Integration of Equation (17)

$$\int dz = \int -\frac{\left(\alpha - \frac{1}{2}\right)K\beta^{n+1}n(-\varepsilon_z)^{n-1}}{\frac{\mu}{2t_0}K\beta^{n+1}(-\varepsilon_z)^n + P_i\frac{\mu(\alpha-1)}{t_0}}d\varepsilon_z \tag{C1}$$

$$\text{Let } a = \left(\alpha - \frac{1}{2}\right)K\beta^{n+1}, \quad b = \frac{\mu}{2t}K\beta^{n+1}, \quad c = \frac{\mu(\alpha-1)}{t}P_i \tag{C2}$$

$$\int dz = \int \frac{an(-\varepsilon_z)^{n-1}d(-\varepsilon_z)}{b(-\varepsilon_z)^n + c} = \frac{a}{b}\int \frac{d(b(-\varepsilon_z)^n + c)}{b(-\varepsilon_z)^n + c} \tag{C3}$$

$$\frac{a}{b}\ln(b(-\varepsilon_z)^n + c) + c_0 = z \tag{C4}$$

The boundary conditions are such that when $z=0$, $\sigma_z=\sigma_r$. By substituting $\varepsilon_z=0$ at $z=0$ into Eq. (C4), the constant c_0 can be determined.

$$c_0 = -\frac{a}{b}\ln(c), \quad z = \frac{a}{b}\ln\left(\frac{b(-\varepsilon_z)^n + c}{c}\right)$$

$$\varepsilon_z = -\left\{\frac{c}{b}\left(\exp\frac{bz}{a} - 1\right)\right\}^{1/n}$$

$$= -\left\{\frac{2(\alpha-1)}{K\beta^{n+1}}p_i\left(\exp\frac{\mu z}{(2\alpha-1)t} - 1\right)\right\}^{1/n} \tag{C5}$$

References

[1] Koc, M., and Altan, T., 2001, "An Overall Review of the Tube Hydroforming (THF) Technology," J. Mater. Process. Technol., **108**, pp. 384–393.

[2] Siegert, K., Häussermann, M., Lösch, B., and Rieger, R., 2000, "Recent Developments in Hydroforming Technology," J. Mater. Process. Technol., **98**(2), pp. 251–258.

[3] Dohmann, F., and Hartl, Ch., 1996, "Hydroforming—A Method to Manufacture Lightweight Parts," J. Mater. Process. Technol., **60**, pp. 669–676.

[4] Nguyen, B. N., Johson, K., and Khaleel, M. A., 2003, "Analysis of Tube Hydroforming by Means of an Inverse Approach," ASME J. Manuf. Sci. Eng., **125**, pp. 369–377.

[5] Asnafi, N., and Skogsgårdh, A., 2000, "Theoretical and Experimental Analysis of Stroke-Controlled Tube Hydroforming," Mater. Sci. Eng., A, **279**(1–2), pp. 95–110.

[6] Asnafi, N., 1999, "Analytical Modelling of Tube Hydroforming," Thin-Walled Struct., **34**(4), pp. 295–330.

[7] Ngaile, G., Jaeger, S., and Altan, T., 2004, "Lubrication in Tube Hydroforming (THF) Part I: Lubrication Mechanisms and Development of Model Tests to Evaluate Lubricants and Die Coatings in the Transition and Expansion Zones," J. Mater. Process. Technol., **146**, pp. 108–115.
[8] Prier, M., and Schmoeckel, D., 1999, "Tribology of Internal High Pressure Forming," MAT-INFO Werksstoff-Informationosgesellschaft mbH, Humburger Allee 26, D-60486 Frankfurt, pp. 379–390.
[9] Ngaile, G., Jaeger, S., and Altan, T., 2004, "Lubrication in Tube Hydroforming (THF) Part II: Performance Evaluation of Lubricants using LDH Test and Pear Shaped Tube Expansion Test," J. Mater. Process. Technol., **146**, pp. 116–123.
[10] Dalton, G., 1999, "The Role of Lubricants in Hydroforming," *Proceedings of the Automotive Tube Conference*, Dearborn, MI, Apr. 26–27.
[11] Koc, M., 2003, "Tribological Issues in the Tube Hydroforming Process—Selection of a Lubricant for Robust Process Conditions for an Automotive Structural Frame," ASME J. Manuf. Sci. Eng., **125**, pp. 484–492.
[12] Gariety, M., 2003, "Enhancement of Tribological Conditions in Tube Hydroforming and the Viability of Twist Compression Test for Screening Tube Hydroforming Lubricants," MS thesis, The Ohio State University, Columbus.
[13] Ngaile, G., Federico, V., Tibari, K., and Altan, T., 2001, "Lubrication in Tube Hydroforming (THF)," Trans. NAMRI/SME, **XXIX**, pp. 51–57.
[14] Ngaile, G., and Altan, T, 2001, "Practical Methods for Evaluation Lubricants for Tube Hydroforming," Hydroforming Journal, pp. 8–12.
[15] Plancak, M., Vollertsen, F., and Woitschig, J., 2005, "Analysis, Finite Element Simulation and Experimental Investigation of Friction in Tube Hydroforming," J. Mater. Process. Technol., **170**, pp. 220–228.
[16] Vollersten, F., and Plancak, M., 2002, "On Possibilities for the Determination of the Coefficient of Friction in Hydroforming of Tubes," J. Mater. Process. Technol., **125-126**, pp. 412–420.
[17] Imaninejad, M., and Subhash, G., 2005, "Proportional Loading of Thick-Walled Cylinders," Int. J. Pressure Vessels Piping, **82**, pp. 129–135.
[18] Jahed, H., Lambert, S. B., and Dubey, R. N., 1998, "Total Deformation Theory for Non-Proportional Loading," Int. J. Pressure Vessels Piping, **75**, pp. 633–642.
[19] Budiansky, B., 1959, "A reassessment of Deformation Theories of Plasticity," ASME J. Appl. Mech., **26**, pp. 259–264.
[20] Varma, N. S. P., and Narasimhan, R., 2008, "A Numerical Study of the Effect of Loading Conditions on Tubular Hydroforming," J. Mater. Process. Technol., **196**, pp. 174–183.
[21] Hwang, Y. M. and Huang, L. S., 2005, "Friction Tests in Tube Hydroforming," Proc. Inst. Mech. Eng., Part B, **219**, pp. 587–593.